



THE UNIVERSITY *of* EDINBURGH

Edinburgh Research Explorer

The performance of leaching experiments to assess the potential mobilization of trace elements during CO₂ injection

Citation for published version:

Wilkinson, M, Carruthers, K, Thomas, ALEX & Haszeldine, S 2020, 'The performance of leaching experiments to assess the potential mobilization of trace elements during CO₂ injection', *Applied geochemistry*. <https://doi.org/10.1016/j.apgeochem.2020.104667>

Digital Object Identifier (DOI):

[10.1016/j.apgeochem.2020.104667](https://doi.org/10.1016/j.apgeochem.2020.104667)

Link:

[Link to publication record in Edinburgh Research Explorer](#)

Document Version:

Peer reviewed version

Published In:

Applied geochemistry

General rights

Copyright for the publications made accessible via the Edinburgh Research Explorer is retained by the author(s) and / or other copyright owners and it is a condition of accessing these publications that users recognise and abide by the legal requirements associated with these rights.

Take down policy

The University of Edinburgh has made every reasonable effort to ensure that Edinburgh Research Explorer content complies with UK legislation. If you believe that the public display of this file breaches copyright please contact openaccess@ed.ac.uk providing details, and we will remove access to the work immediately and investigate your claim.



1 The performance of leaching experiments to assess the potential mobilization of trace elements
2 during CO₂ injection

3 Mark Wilkinson, Kit Carruthers, Alexander L. Thomas, R. Stuart Haszeldine

4 School of GeoSciences, Grant Institute, The King's Buildings, James Hutton Road, Edinburgh EH9 3FE,
5 UK

6 Corresponding author: Mark Wilkinson, mark.wilkinson@ed.ac.uk

7

8 ABSTRACT

9

10 To control reservoir pressure during CO₂ injection for Carbon Capture and Storage, it may be
11 necessary to produce native porewaters to the surface. These porewaters could contain potentially
12 toxic metals mobilised from the reservoir rock by the injected CO₂, which would then be discharged
13 into the ocean if offshore, or treated if onshore. To evaluate the risk, both chip and grain samples
14 from a UK North Sea sandstone that is a candidate for CO₂ storage were exposed to CO₂-saturated
15 water in 30 day leaching experiments, and the metal load of the porewaters was analysed. Only Pb
16 and Zn were convincingly mobilised (median 30 vs 2 µg/L for Pb; 130 vs 25 µg/L for Zn), and these
17 elements these have been previously reported to be more easily mobilised in experiments than
18 during in-situ CO₂ injection. Hence, in this case, the risk of releasing toxic metals into the
19 environment is assessed as small, and comparable to existing hydrocarbon operations. Results are
20 significantly variable within a single sandstone reservoir, suggesting that experiments with multiple
21 samples are required to make a realistic assessment of leaching potential. An assessment of other
22 potential chemical data for assessing trace metal leaching suggested that only the comparatively
23 lengthy leaching experiments generated useful data.

24

25 **1. Introduction**

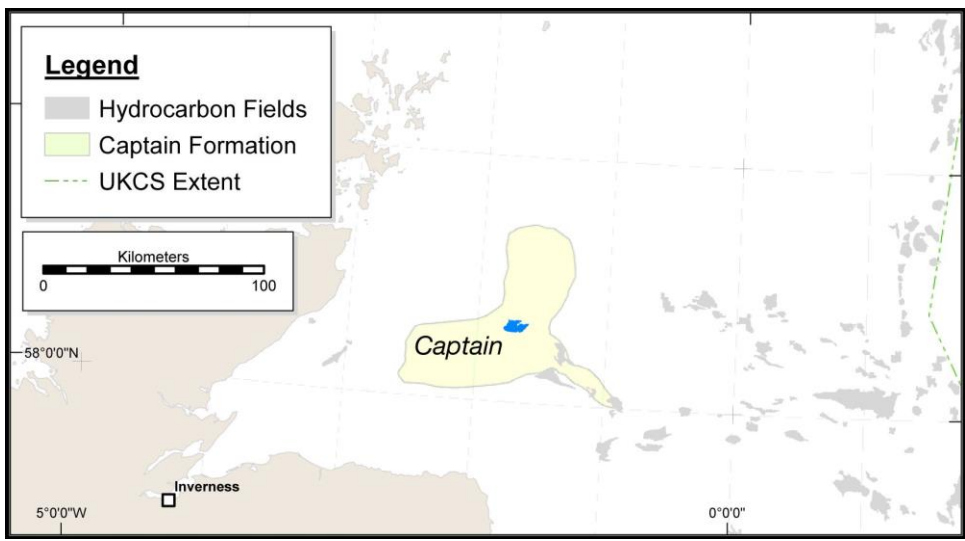
26

27 Carbon capture and storage technology is being implemented at industrial scale in several locations
28 worldwide. Finding sufficient secure storage is essential, and a limiting factor in the storage capacity
29 of many sites will be the build-up of porewater pressure during injection (e.g. SCCS, 2011). One
30 solution to control subsurface pressure, and hence to increase storage capacity, is to produce
31 porewater from the reservoir to the surface (SCCS, 2011). This porewater could potentially contain
32 some dissolved CO₂, although the return of CO₂ back to the surface will obviously be kept to an
33 absolute minimum. Potentially toxic trace metals may have been mobilised from the reservoir rock
34 into the porewater, which will require safe disposal. There are now multiple papers focused on CO₂ –
35 water - rock interactions with respect to underground CO₂ storage, and the potential environmental
36 impacts. The published literature encompasses modelling, laboratory, and field experiments, with
37 environmental impacts of CO₂ leakage on groundwater quality considered in more recent
38 publications (e.g. Kirsch et al. 2014; Lu et al. 2014; Zheng and Spycher, 2018). Field studies have also

39 focused on the environmental impacts of CO₂ release into underground supplies of potable water
40 as an aid to understanding in-situ reactions (e.g. Cahill et al. 2013; Trautz et al. 2013), as opposed to
41 often far-from-equilibrium laboratory experiments.

42

43 This paper deals with the Captain Sandstone Member of the Moray Firth of Scotland (Fig. 1) which
44 has been extensively studied previously as a site for the engineered storage of CO₂. A report
45 commissioned by the UK government identified a portion of the sandstone, known as the Captain X
46 site, as one of the 5 most promising CO₂ storage sites on the UK Continental Shelf (UKCS; Pale Blue
47 Dot Energy, 2016). The storage capacity of the site was estimated as 60 Mt CO₂ (Pale Blue Dot
48 Energy, 2016). Earlier work on the same sandstone member concluded that the capacity of the
49 entire sandstone (as opposed to the geographically-restricted Captain X site) varied from 358 to
50 1668 Mt CO₂, depending on assumptions about the geometry, geomechanical properties of the
51 reservoir and the nature of the boundaries of the sandstone (SCCS, 2011). A key finding was that, for
52 maximum storage capacity, large volumes of porewater from the reservoir might have to be
53 produced to the surface, and disposed of, most probably by discharging into the sea ('over-
54 boarding'). To reduce the uncertainty in storage capacity, and hence the risk of investment in a CCS
55 project in the Captain Sandstone Member, it would likely be necessary to plan for the production of
56 porewaters to the surface, even though it may not be needed. The environmental risks of such a
57 strategy must hence be evaluated, even though every effort would be made to avoid the production
58 of CO₂-laden waters back to the surface, as this would defeat the purpose of injection.



59

60 Fig. 1 – Location map showing the extent of the Captain Sandstone Member (yellow), and the
61 Captain hydrocarbon field (blue).

62

63 In this study, experimental work under controlled laboratory conditions that are representative of
64 reservoir temperatures has been carried out to determine how reservoir rocks from the Captain
65 Sandstone Member react when CO₂ is introduced. Our results are compared to a database of bi-
66 annually reported metal concentrations (As, Cd, Cr, Cu, Pb, Hg, Ni and Zn) in produced waters
67 associated with hydrocarbon production from the Captain Sandstone Member. These monitoring

68 data were compiled since 2006 as required for some permits for hydrocarbon production in the
69 Environmental and Emissions Monitoring System (EEMS, [https://www.gov.uk/oiland-gas-eems-](https://www.gov.uk/oiland-gas-eems-database)
70 [database](https://www.gov.uk/oiland-gas-eems-database); obtained January 2015). This allows for the comparison of the experimental results to
71 analyses of porewaters routinely discharged into the North Sea during oil industry operations
72 utilising the same reservoir sandstone. It is assumed here that the EEMS analyses are representative
73 of the in-situ porewaters in the subsurface, henceforth called the native porewaters.

74

75 The Captain Sandstone Member is a Lower Cretaceous mass-flow sandstone-dominated unit of up to
76 200 m thickness (Pinnock et al., 2003) covering c. 4000 km² (from maps in SCCS, 2011). The
77 sandstone forms the reservoir for several commercial hydrocarbon fields, including the Captain
78 Field. The porewaters within the Captain Sandstone Member are below seawater salinity (12 –
79 25,000 ppm TDS; Pinnock et al., 2003), and have been routinely discharged into the North Sea during
80 hydrocarbon production. The Captain Sandstone Member in the Blake Field, the source of the
81 experimental samples, is reported to be at 56°C and c. 330 bars pressure (Melvin et al., 2008),
82 representing a significant overpressure.

83

84 **2 Materials & methods**

85

86 The study rock is hydrocarbon reservoir core from the Blake Field borehole 13/24a-4 (Table 1),
87 drilled in December 1997 to January 1998. The sandstone samples were collected from the UK
88 national collection stored by the British Geological Survey. Both samples were characterised using
89 thin-sections impregnated with a blue-dyed resin examined with a petrographic microscope.
90 Porosity and mineral abundance were determined by point-counting 200 points per thin-section in a
91 grid pattern. Phases recognized during the thin section analysis but not recorded in the point
92 counting have been recorded as present in quantities < 1%. Sample SA7 was oil stained and smelled
93 of oil, while sample SA10 had no obvious oil contamination. Grain size was determined using a
94 calibrated graticule on the microscope eyepiece.

95 *2.1 Leaching experiments and water analysis*

96 Rock samples were introduced to the reaction vessels as either chips of approximately 1 cm
97 diameter, or as disaggregated grains. Sample preparation used a geological hammer and mortar and
98 pestle; disaggregation required minimal force due to the low degree of consolidation of the material.
99 Samples were added at the weights given in Table 1, to 250 mL of brine of 13,500 mg / L salinity
100 made using Fisherbrand 'SLR' grade sodium chloride solid reagent and 11 mΩ /cm high purity water
101 from a Milli-Q water system. The NaCl has < 0.5 ppm of relevant specified impurities (Cu, Pb and Zn)
102 which equates to less than 10 ppb in solution, significantly below the limit of analytical detection. It
103 is assumed that the elements of interest that are not in the manufacturer's specification are present
104 in equally low concentrations. The reaction vessels were held at atmospheric pressure and a target
105 temperature of 56 °C, with measured fluctuation between c. 55 and 58 °C and extremes of 50 – 68
106 °C, for 30 days. Blank samples, i.e. with no rock, were run both with (CAP_F1) and without (CAP_B1)
107 CO₂. Although the partial pressure of oxygen within the vessels was presumably somewhat lower

108 than the surrounding atmosphere, the conditions were still oxidising. No attempt was made to
109 reproduce reducing conditions as might be anticipated in the subsurface.

110 Table 1. Batch experiment configurations. CO₂ flow refers to the presence (Y) or absence (N) of
111 bubbled CO₂ in the experiment.

Sample Name	Sample depth (DD m)	Sample type	Sample Weight (g)	CO ₂ Flow
CAP_F1		blank	0	Y
CAP_SA7_F2	1620	chip	3.36	Y
CAP_SA7_F3	1620	grain	2.75	Y
CAP_SA10_F4	1656	chip	3.36	Y
CAP_SA10_F5	1656	grain	2.64	Y
CAP_B1		blank	0	N
CAP_SA7_B2	1620	chip	3.17	N
CAP_SA7_B3	1620	grain	2.75	N
CAP_SA10_B4	1656	chip	3.18	N
CAP_SA10_B5	1656	grain	2.85	N

112

113 The batch reaction vessels were Quickfit™ 250 mL round bottomed, three necked borosilicate flasks
114 with Liebig condensers. Prior to set up, all glassware and sampling vessels were soaked in a 10%
115 nitric acid bath for at least 12 hours, rinsed with distilled and deionised water (11 mΩ / cm), and air
116 dried. Glassware was then wrapped in aluminium foil and dried at 450° C for four hours to destroy
117 any residual organic material, and left wrapped in the foil until the experiment was set up. Dry CO₂
118 gas was fed to each flask where appropriate from a BOC vapour withdrawal CO₂ bottle with attached
119 2 bar regulator, to glass injection tubes. CO₂ flow was regulated using Hoffman tubing clamps to
120 maintain a pressure of 1.4 bar to bubble CO₂ into the batch fluids. Fluid samples were drawn from
121 the batch flasks using a pipette and passed through a 0.22 µm filter into PTFE sample bottles,
122 acidified to 2% v / v with analytical grade 69 % HNO₃ and refrigerated prior to analysis. Results were
123 obtained for 3 categories of experiment: blanks (no rock, with or without CO₂); rock plus added CO₂,
124 henceforth referred to as +CO₂ experiments; and controls i.e. rock with no added CO₂. Solution
125 composition during the experiments was modelled using PHREEQC v3.3.3 using mineralogy from X-
126 ray diffraction (see below) and the database Phreeqc.dat. The fluid was modelled as either saturated
127 with air, or with CO₂ as appropriate.

128 Batch fluid samples were analysed by ICP-MS for major and trace elements using an Agilent 7500ce
129 with octopole reaction system, employing an RF forward power of 1540 W, reflected power of 1 W,
130 argon gas flows of 0.82 L/min and 0.2 L/min for carrier and makeup flows, respectively, and nickel
131 skimmer and sample cones, with a Micro mist nebuliser and peristaltic pump providing a solution
132 uptake rate of approximately 1.2 mL/min. The instrument was operated in spectrum multi-tune
133 acquisition mode and three replicate runs per sample were employed. Calibration was with Merck VI
134 multi-element ICP standard with the exception of Hg, which was calibrated with a BDH 'Spectrosol'
135 ICP-MS standard, and Cs, P, Sb, Si, Sn, Th, Ti and Zr which were calibrated with SPEX Certiprep R or
136 Fisherbrand ICP-MS standards. All standards were made up with the same NaCl concentration as the
137 samples to be analysed.

138 Zero values in the experimental data refer to concentrations less than the analytical limit of
 139 detection (LOD; Table 2). As calculated mean concentrations are dependent on the LOD, median
 140 values are quoted which are independent of the LOD, except in the case that the median value is the
 141 LOD e.g. for Cd. The LOD was calculated using analyses of 10 blank aliquots of sample matrix and 2%
 142 HNO₃ solutions. The instrumental LOD was calculated as 3σ of the blanks' ICP-MS counts per second
 143 divided by the slope of calibration line (Vandecasteele and Block, 1993). Concentrations of elements
 144 in the blank flasks (which had no rock samples) are assumed to be representative of any background
 145 concentrations of elements present in the fluid samples. As the majority of these were below
 146 detection limits no correction was made the experimental data for background levels of
 147 contamination. Detection limits are not published for the EEMS dataset.

148 The mass of element mobilised during the leaching experiments was calculated using the measured
 149 concentrations multiplied by the volumes of fluid extracted from the flasks for each measurement.
 150 For concentrations below the limit of detection, a value equal to the limit of detection was assumed,
 151 to produce a 'worst-case' maximum value for the quantity of element mobilised.

152

153 Table 2 – Detection limits (LoD) for by ICP-MS trace elements

Element	LoD µg / L	Predicted no-effect concentrations* µg / L	Seawater concentration µg / L
As	0.26	0.6 + Cb	0.75 – 4.0; Cutter et al. (2001)
Cd	0.005	0.2 + Cb	0.00 – 0.11; Middag et al. (2018)
Cr	0.08	0.6 + Cb	0.10 – 0.21; Jeandel and Minster (1987)
Cu	2.9	2.6	0.00 – 0.32; Boiteau et al. (2016)
Hg	0.02	0.05 + Cb	0.00 – 0.50; Bowman et al. (2015)
Ni	0.04	8.6 + Cb	0.12 – 0.47; Schlitzer et al. (2018)
Pb	0.13	1.3	0.00 – 0.01; Schlitzer et al. (2018)
Zn	1.8	3.4 + Cb	0.00 – 0.52; Wyatt et al. (2014)

154 * Cb = background concentration; OSPAR Commission (2014)

155 pH was measured by drawing 5 mL of fluid from the batch flasks using pipettor, transferring to a,
 156 rinsed, acid cleaned vial, cooling in air to approx. 26 - 27°C and analysing with a Hanna HI9125 pH
 157 meter with attached glass VWR ceramic junction pH electrode, calibrated with Hanna HI7007 (pH
 158 7.01) and HI7004 (pH 4.01) NIST traceable buffer solutions, accurate to ± 0.01 pH. Due to degassing
 159 of CO₂ during cooling of the samples, the pH data are not regarded as being very reliable.

160

161 Alkalinity was measured as bicarbonate (mg/L) using a Palintest Photometer 7100, accurate to ± 5
 162 mg/L and with a 2σ repeat measuring precision of 5.7 %. Measurements were taken by crushing a
 163 Palintest alkophot 'M' reagent tablet in 9 mL of sample, immediately after removal from the batch
 164 flask. The photometer was calibrated with a blank of 9 mL of NaCl solution of the same
 165 concentration as the synthetic batch fluids. For the majority of the pH values obtained for the
 166 experiment (4.8 - 8.5 for non-blank experiments), bicarbonate is the dominant carbonate species
 167 and therefore a reasonable proxy for total alkalinity.

168 *2.2 Bulk rock geochemistry*

169 Bulk chemical analysis of the sandstone samples was carried out by complete dissolution of sample
170 SA7 (insufficient sample SA10 remained) by microwave acid digestion using the following procedure.
171 Four mL of concentrated HF, 3 mL concentrated HNO₃ and 2 mL 30 % HCl were added. In a CEM
172 Mars Xpress system, a set of 24 samples including procedural blanks and 2 soil standard reference
173 materials (NIST SRM2710a and SRM2711a) were digested in closed vessels at 200 °C for at least 30
174 minutes. The digested samples were evaporated to near dryness in the microwave system, using a
175 MicroVap accessory. Samples were then taken up in the microwave in 10.5 ± 0.3 mL 2% HNO₃, at
176 180 °C. The resulting solution was analysed by ICP-MS as above. Uncertainties were calculated from
177 three repeated analyses of the sample. Due to the microwave digestion method employed, Si
178 volatilises as hexafluorosilicic acid and therefore Si was not determined.

179 *2.3 Sequential extraction procedure*

180 A sequential extraction procedure (SEP) was performed on sample SA7 using a modified version of
181 the method presented by Wigley et al. (2013) to include an additional step to target sulphide
182 mineral phases, which replaced the hydrochloric acid step. Sample and reagent masses and volumes
183 were taken from Tessier et al. (1979). 10 g each of sample were crushed with a mechanical jaw
184 crusher and the resulting chips ground to a powder with a tungsten-carbide mill. Samples were
185 homogenised and 1,000 ± 2 mg transferred to 50 mL centrifuge tubes. Reagents were added to the
186 centrifuge tubes in the steps listed below.

187 1. Water: 8 mL 18.2 MΩ de-ionized (D.I.) water with continuous agitation for 2 hours.

188 2. Exchangeable fraction: 8 mL 1M sodium acetate solution at pH 8.2, with continuous agitation for 3
189 hours.

190 3. Carbonates: 8 mL 1 M sodium acetate adjusted to pH 5 with acetic acid, with continuous agitation
191 for 7 hours, repeated 3 times with fresh reagent.

192 4. Oxides: 8 mL 0.1 M ammonium oxalate buffer adjusted to pH 3 with oxalic acid. Occasional
193 agitation for 54 hours, repeated 3 times with fresh reagent.

194 5. Sulphides: 3 mL 0.02M nitric acid + 5 mL of 30% hydrogen peroxide adjusted to pH 2 with
195 concentrated HNO₃, heated to 85 °C in a water bath for 2 hours with occasional agitation.

196 Added 3 mL hydrogen peroxide, adjusted to pH 2 with nitric acid, and heated again for 3 hrs. After
197 cooling to approximately room temperature, 5 mL of 3.2 M ammonium acetate in 20% (v/v) nitric
198 acid was added and the whole mixture diluted to 20 mL with D.I. water before continuous agitation
199 for 30 mins.

200 6. Bulk digestion / silicates: Microwave digestion as above.

201 All continuous agitation was carried out by means of a rotating 'end-over-end' shaker connected to a
202 voltage controller to adjust rotating speed. With the exception of Step 5, all SEP steps were carried
203 out at a room temperature of c. 21 ° C. After each extraction period the samples and supernatants
204 were centrifuged at 12,000 rpm for 20 minutes, and the supernatants removed from the centrifuge
205 tubes by carefully pouring out into an acid cleaned vial. This centrifugal speed was higher than the

206 Wigley et al. (2013) method as their speed was not sufficiently high to ensure that any clays in
 207 suspension in the supernatant 'plate out' during centrifugation. Although the clays plated out at the
 208 higher centrifugal speed used in this work, nonetheless when the supernatants were removed, some
 209 of the finest solid material was re-suspended and transferred into the sub-sampling vial. This was
 210 most pronounced after the first step using deionised water and became less apparent throughout
 211 the remainder of the steps. Each supernatant was filtered through a 0.22 μm filter into the final
 212 sampling vessel. Each sample was acidified with 2% nitric acid and refrigerated for preservation until
 213 analysis.

214 Bulk mineral analysis was carried out using a Bruker D8-Advance X-ray Diffractometer, employing a
 215 2-theta (2θ) configuration, with X-rays generated by a Cu-anode X-ray tube operating at 40 kV, and a
 216 tube current of 40 mA. Diffracted X-rays were detected using a Sol-X energy dispersive detector,
 217 scanning from 2° to 60° 2θ at a scan rate of $0.01^\circ/\text{second}$ and the resultant diffractograms compared
 218 with the 2008 issue of the International Centre for Diffraction Data (ICDD) diffractogram database
 219 library using the EVA analysis package. The uncertainty in the analyses is calculated by the software.
 220 The detection limit for crystalline phases is approximately 1 wt %, with values of less this indicative
 221 of probable presence only.

222

223 3. Results

224 Table 3 summarises the petrography of the samples. The samples were only poorly consolidated,
 225 with very few occurrences of brittle deformation of framework grains. There was visible dissolution
 226 and alteration to kaolinite of some feldspars and minor chloritization of a lithic fragment. Thin green
 227 rims that could not be identified optically were observed on some grain surfaces in SA7. No cement
 228 was observed in SA10. A minority of grains are replaced by microcrystalline calcite. Both samples are
 229 sub-arkoses according to the classification of Folk (1974).

230 Table 3 – Sample petrography

	SA7 point count	SA7 XRD / wt %	SA10 point count	SA10 XRD/ wt %
Max grain size	1.2 mm		1.8 mm	
Min grain size	0.05 mm		0.006 mm	
Grain size	fine-medium sand		medium sand	
Sorting	moderate		moderate	
Roundness	angular to well rounded		sub-angular to well rounded	
Porosity	30 %		30	
Quartz	84	81 ± 1	82	88 ± 1
Feldspars	12	9 ± 1	16	5 ± 1
Biotite	<1		<1	
Muscovite / illite	1	3.3 ± 0.5	2	2.1 ± 0.5
Calcite	<1	1.6 ± 1.4	<1	0.4 ± 0.1
Kaolinite	<1	2.8 ± 0.6		0.9 ± 0.2
Chlorite		0.3 ± 0.3		3 ± 0.5
Glauconite	2		<1	

Opaque	1		<1	
Oxides/Hydroxides	<1		<1	
Zircon	<1			
Corundum	<1			0.7 ± 0.1
Anatase				1.0 ± 0.1
Lithic fragments			<1	
Halite		2.2 ± 0.1		

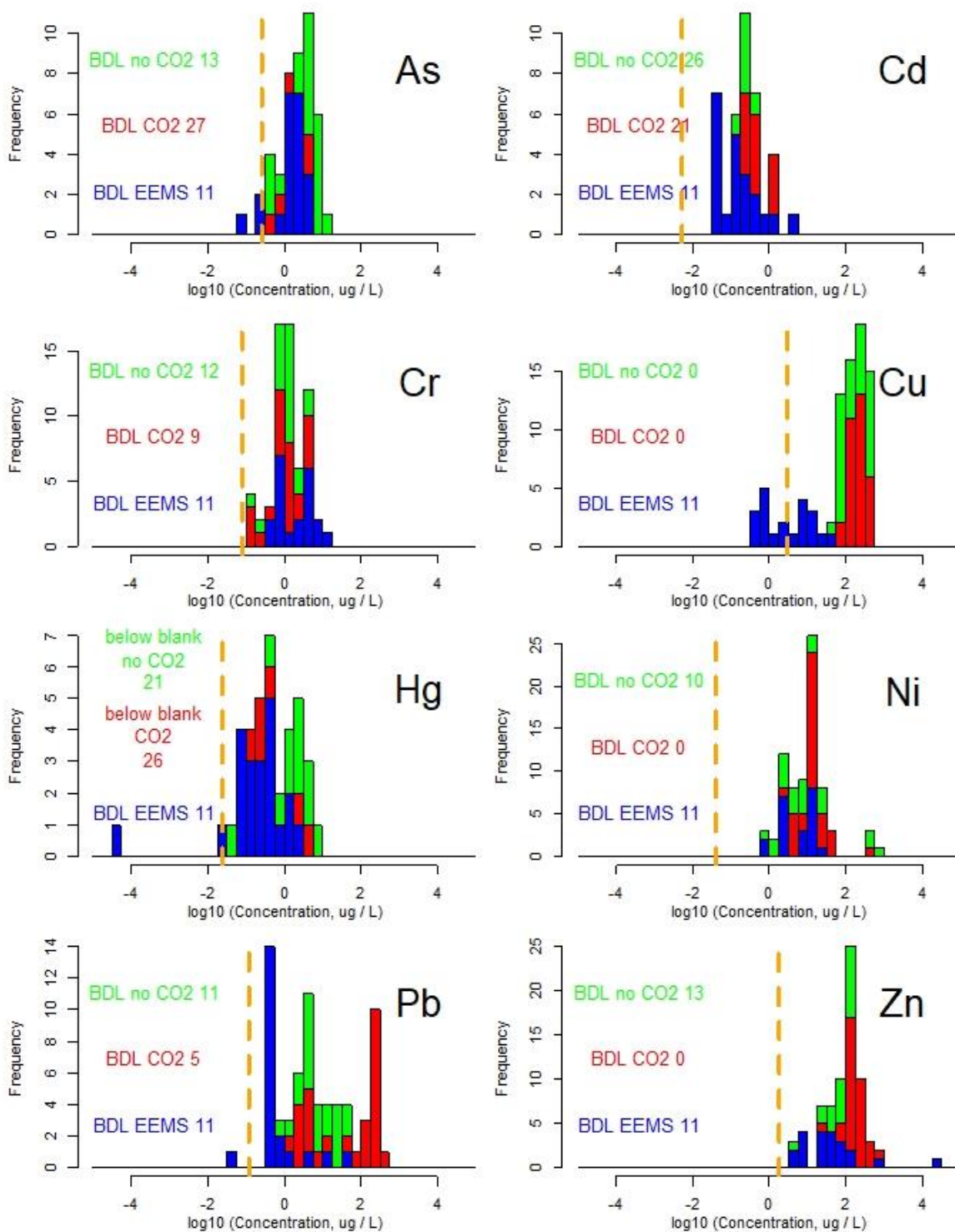
231

232 Porewater composition from the batch experiments are in Tables 4A and B. Figure 2 shows trace
 233 metal concentration for the EEMS database and the batch reaction experiments for both the
 234 controls and the CO₂ - experiments. Note that a substantial proportion of the experimental analyses
 235 are below the limit of detection (BDL; Fig. 2), and are shown as '0' in Tables 4A and B. Analyses
 236 below detection limits are not plotted on Fig. 2 but the numbers of such data are shown. Note that
 237 approximately one half of the analyses are below detection limits (0 – 90 % for an individual
 238 element; overall mean 57 ± 8 %). For most of the trace elements, the blank concentrations are
 239 significantly lower than the experimental concentrations. However, for Hg, the blank concentrations
 240 are comparable in magnitude to the experimental concentrations. For this reason, the Hg data in Fig.
 241 2 are blank-corrected, i.e. the average blank analysis has been subtracted from the experimental
 242 analysis for the same day for which samples were collected.

243

244 The range of trace element concentrations for the experiments are similar to those of the EEMS data
 245 for As (median BDL [0.26 µg/L] with CO₂; 2.4 µg/L without CO₂; EEMS 1.0 µg/L), Cr (median 0.5 µg/L
 246 with CO₂; BDL [0.08 µg/L] without CO₂; EEMS 0.7 µg/L), Hg (blank-corrected; median BDL [0.02 µg/L]
 247 with CO₂; BDL without CO₂; EEMS 0.08 µg/L) and Ni (median 7.5 µg/L with CO₂; 1.7 µg/L without CO₂;
 248 EEMS 3.0 µg/L). Element concentrations in the leaching experiments are substantially higher than
 249 the EEMS data for Cu (median 100 µg/L with CO₂; 90 µg/L without CO₂; EEMS 0.8 µg/L), Pb (median
 250 30 µg/L with CO₂; 2 µg/L without CO₂; EEMS 0.5 µg/L) and Zn (median 130 µg/L with CO₂; 25 µg/L
 251 without CO₂; EEMS 9 µg/L). The experimental data for Cd appears to be higher (Fig. 2; median value
 252 with CO₂ is BDL [0.005 µg/L]; without CO₂ is BDL; EEMS 0.05 µg/L) but 21 out of 32 analyses were
 253 below detection limit in the +CO₂ experiments, so that overall the experimental data and the EEMS
 254 data are comparable, or the +CO₂ experimental data may in fact be lower. A more quantitative
 255 analysis is not possible given that the values of the analyses below detection limit are not known.
 256 For Cu, the median of experiments is 90 - 100 µg/L, much higher than 0.8 µg/L for the EEMS data.
 257 However for Cu both experiments with and without CO₂ have similar median values (90 versus 100
 258 µg / L respectively). Hence, the only elements for which the CO₂ appears to have significantly
 259 increased the trace element concentrations are Pb and Zn.

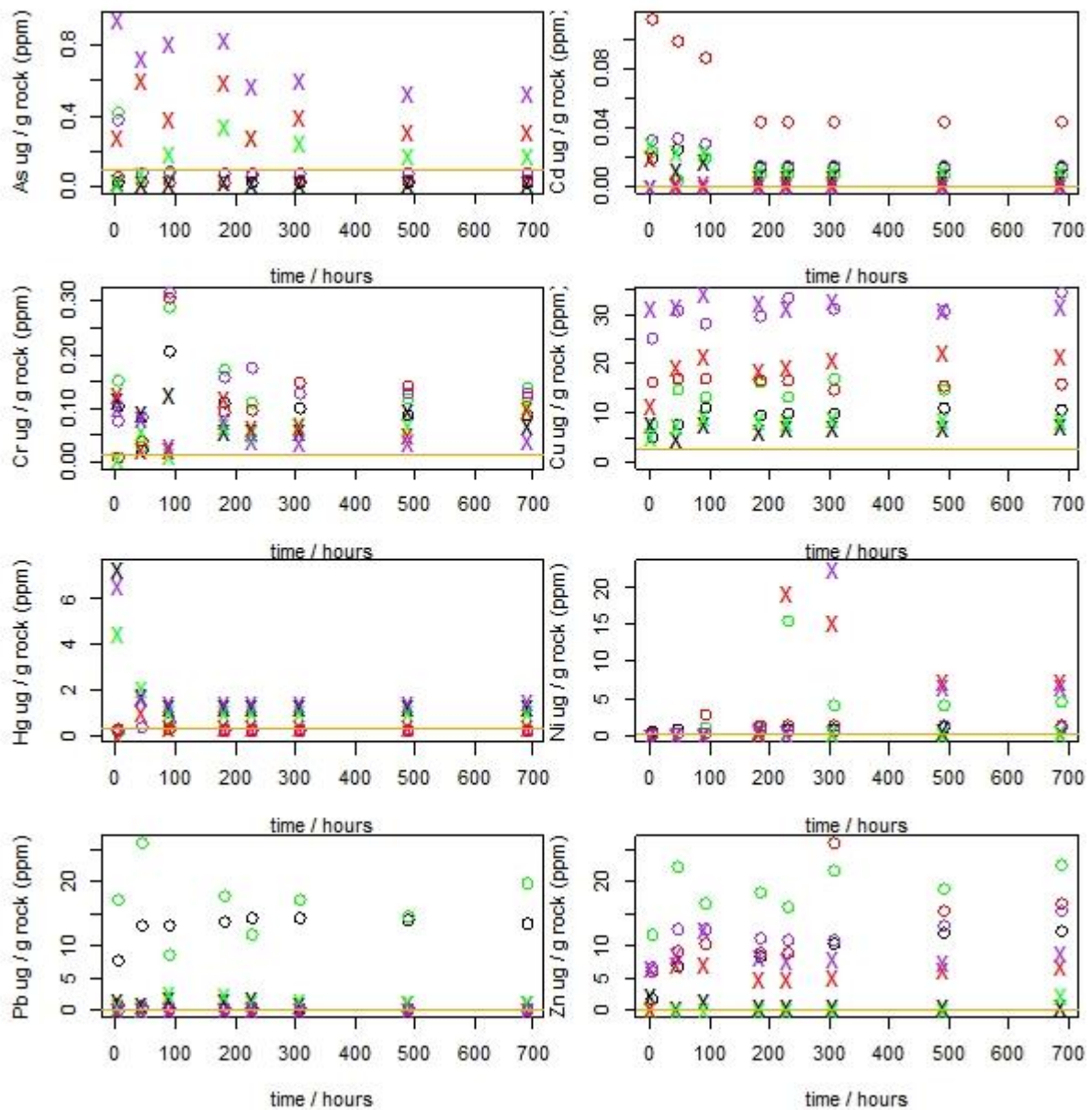
260



261

262 Fig 2 – Comparison of trace elemental concentrations from lab experiments and porewater from the
 263 Captain Sandstone Member (EEMS database). The data that fall below the limit of detection (the
 264 orange dotted line) are not plotted; the numbers of analyses that fall below this are given as below
 265 detection limit (BDL). Green is experimental data with no added CO₂, red is experimental data with
 266 added CO₂, blue is the EEMS dataset.

267 A time sequence of calculated trace element mass per g rock is shown in Fig. 3. Concentrations of
 268 arsenic are higher in the $-CO_2$ flasks than in those with added CO_2 . In the majority of the
 269 experiments, the leached metal concentrations appear to have stabilised by the end of the
 270 experiments, i.e. to have reached an approximately constant value, or to be decreasing. The water-
 271 extractable metal loads determined on sample SA7 (shown as horizontal lines on Fig. 3) are not
 272 generally close to the leached loads for the same sample, with the possible exceptions of As, Hg for
 273 the $+CO_2$ experiments and Ni for the $-CO_2$ experiments.



274
 275 Fig. 3 – Calculated quantities of trace elements released from rock leaching experiments, through
 276 time, see methods section for details. Crosses are controls (no added CO_2), circles are with CO_2 . Each
 277 colour represents a single experimental run. The horizontal orange lines are the concentrations from
 278 the water stage of the selective extraction procedure for sample SA7.

279

280 pH of the solutions varied from 3.9 - 5.4 for the blank flasks with added CO₂; 4.7 – 8.3 for blanks
281 without added CO₂; 4.8 - 8.4 for flasks with rock sample and added CO₂; and 5.2 to 8.5 for flasks
282 with no rock and added CO₂ (Tables 4A and B). Alkalinity values for the two blank flasks show a
283 relatively small effect from the addition of CO₂, with values approximately constant through the
284 duration of the experiment at 25 - 65 mg / L (blank +CO₂) and 20 - 70 mg / L (blank, -CO₂). Alkalinity
285 values for sample SA7 without the addition of CO₂ are only slightly higher than the blanks at a range
286 of 45 - 95 mg / L, while SA10 values without the addition of CO₂ increase from 80 mg/L to 165 mg/L.
287 The addition of CO₂, however, increases alkalinity concentrations for both samples SA7 and SA10,
288 with SA7 values increasing from 105 mg / L to 290 mg / L, and SA10 increasing from 135 mg / L to
289 500 mg / L (Tables 4A and B). The DIC of the solution during the experiments was modelled using
290 PHREEQC as 0.024 mol / L assuming no reactants other than CO₂ and water, and as 0.036 mol / L
291 with calcite present.

292 Bulk analysis of sample SA7 (Table 5) showed that of the 8 trace metals of interest, concentrations
293 are generally < 10 ppm, with Cr and Zn being the (slight) exceptions. Cadmium concentrations are
294 very low at 0.029 ppm. Results of the selective extraction procedure are in Table 6 and the water
295 extraction stage is in Table 5 for the 8 trace metals. The mean proportion of the total elements
296 leached in the experiments is very variable (Table 5), from a small fraction of the total in the bulk
297 rock analysis (< 1 %; Cd, Cr) to greater than 50 % (Pb, Cu, Zn). As, Ni and Hg are intermediate.

298

299

300 Table 5: Bulk analysis of sample SA7 by ICP-OES unless indicated, and trace metals leached during
 301 experiments and the water stage of the selective extraction procedure (SEP).

Element	Whole rock concentration $\mu\text{g/g}$	2σ (n = 3)	Element leached $\mu\text{g/g}$ rock			Water stage of the SEP
			range	mean -CO ₂	mean +CO ₂	
Al	20,000	2,000				
As	4.3	0.7	0.02 – 1	0.32	0.07	0.1 ± 0.008
Ba	640	60				
Ca	5600	800				
Cd (ICP-MS)	160	0.001	0.0004 – 0.1	0.007	0.03	0.0008 ± 1e-5
Cr	24	3	0.006 – 0.3	0.067	0.13	0.013 ± 0.001
Cu	7.8	0.8	5 - 35	17	17	2.5 ± 0.1
Fe	5400	700				
Hg (ICP-MS)	5.9	1.2	0.1 - 130	1.5	0.27	0.3 ± 0.003
K	14100	800				
Li	14	2				
Mg	940	80				
Mn	54	7				
Na	6200	500				
Ni	5.9	0.7	0.003 – 23	2.9	1.7	0.25 ± 0.003
Pb	6.6	0.9	0.01 - 26	0.8	7.6	0.008 ± 0.0009
Ti	1500	200				
U	7.5	0.7				
Zn	16	2	0.2 - 26	3.9	13	0.11 ± 0.002

302

303 Results of X-ray diffraction (XRD) analysis of the unreacted rock samples (SA7 and SA10) are given in
 304 Table 3, as weight %. Values of less than 1 % are indicative only of probable presence of a mineral in
 305 the sample. Fe-oxides were not detected, neither were they positively identified in thin-section
 306 using a petrographic microscope. However, thin green rims that could not be identified optically
 307 were present on some grain surfaces in SA7, and these could include Fe-oxides. Geochemical
 308 evidence (see below) suggests that Fe-oxides are present, presumably in concentrations below
 309 detection limit for XRD.

310

311 Table 6: Results of the selective extraction procedure, units $\mu\text{g/g}$.

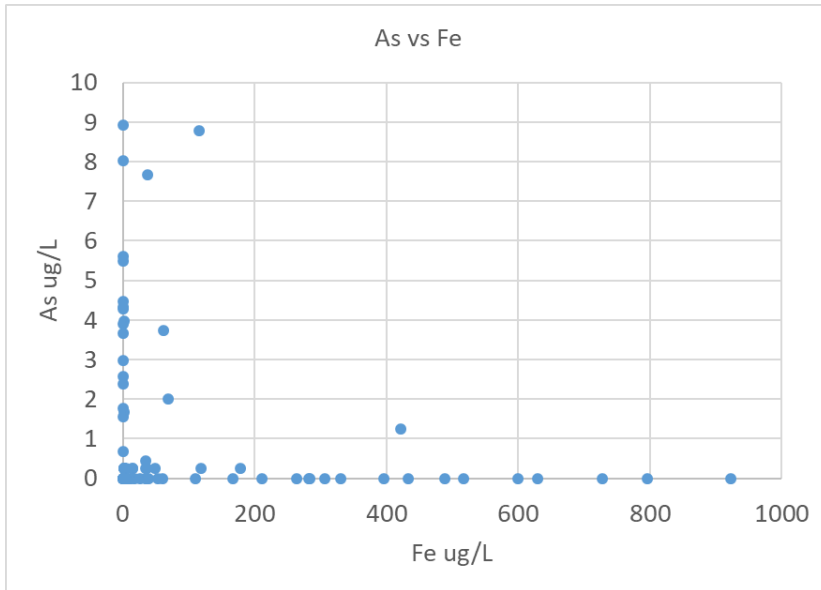
Element	Extraction stage						
	Water	Exchangeable	Carbonate	Oxide	Sulphide	Silicate	Bulk
Al	0	0	0.350	0	0	0	0
As	1.192	0	0	0.434	0	0	0

Ba	0	0.035	0	0.238	0.045	0	0
Ca	0	35.167	6.183	0	0	130.675	130.675
Cd	0.041	0.028	0	0	0	0.175	0.175
Cr	0.462	0.074	0	0	0	2.900	2.900
Cu	0.351	3.104	11.741	0	2.704	1.725	1.725
Fe	14.985	0	16.477	0.071	1.180	0	0
Hg	0	0	0.010	0.015	0.038		
K	0	45.850			0	0	0
Li	0.416	0	0	0	0	4.925	4.925
Mg	0.638	0.501	1.407	0	0.352	87.300	87.300
Mn	0	0.056	0.062	0	0	0	0
Na	83.075					568.475	568.475
Ni	0	1.137	0.809	1.381	2.109	0	0
Pb	0.174	0.103	0.039	0.012	0.040	0	0
Ti	0.280	0	0	0.011	0	0	0
U	0.028	0	0.000	0	0	0	0
Zn	1.283	3.369	0.547	0.158	2.475	10.075	10.075
<i>n</i> =	6	6	18	18	6	4	4

312

313 4. Discussion

314 The only metal with a strong decrease in concentration in the presence of CO₂ was arsenic (Fig. 3;
315 median BDL [0.26 µg/L] with CO₂; 2.4 µg/L without CO₂). A relationship between Fe and As is
316 demonstrated by Fig. 4, where As concentrations are only above c. 1 µg/L in solutions with low (<
317 100 µg/L) Fe. As arsenic (V) absorption onto Fe-oxides increases strongly with decreasing pH (e.g.
318 Hsia et al., 1994), a simple pH control can be proposed. Any Fe-oxides could be an original
319 component of the rock (perhaps the green rims on some grains in sample SA7); or formed by the
320 oxidation of pyrite during the experiments; or during the storage of the core in the approximately 15
321 years between drilling and sampling. The latter is feasible, as pyrite is prone to reaction to oxy-
322 hydroxides even in museum collections. The general decrease in As concentration during the
323 experiments (e.g. c. 9 – 4 µg/L in experiment CAP_SA10_B5) could be interpreted as the progressive
324 reaction from pyrite to Fe-oxides, increasing the surface area available for adsorption, or that
325 adsorption is a slow reaction on the time scale of the experiments. Note that, although no sulphide
326 minerals were detected by XRD analysis, the sulphide stage of the selective extraction procedure did
327 generate metal concentrations above analytical detection limits that were dominated by iron, as
328 might be expected if pyrite were present. The measured 260 µg / g of Fe liberated by the sulphide
329 stage of the selective extraction procedure (Table 6) equates to c. 0.05 % pyrite, comparable to the
330 0.03 % of Allen et al. (2020, their Fig. 6) using QUEMSCAN analysis of a thin section of the Captain
331 Sandstone, well below the detection limit for XRD. At least some of the remainder of the whole-rock
332 Fe could be present as Fe-oxide coatings to detrital grains, however chlorite has a significant Fe
333 content and is probably present in both rock samples (the 0.3% in SA7 is only an indicator of possible
334 presence). Given the low abundance of chlorite (0.3 – 3 wt %), then separation for chemical analysis
335 is considered to be impractical.



336

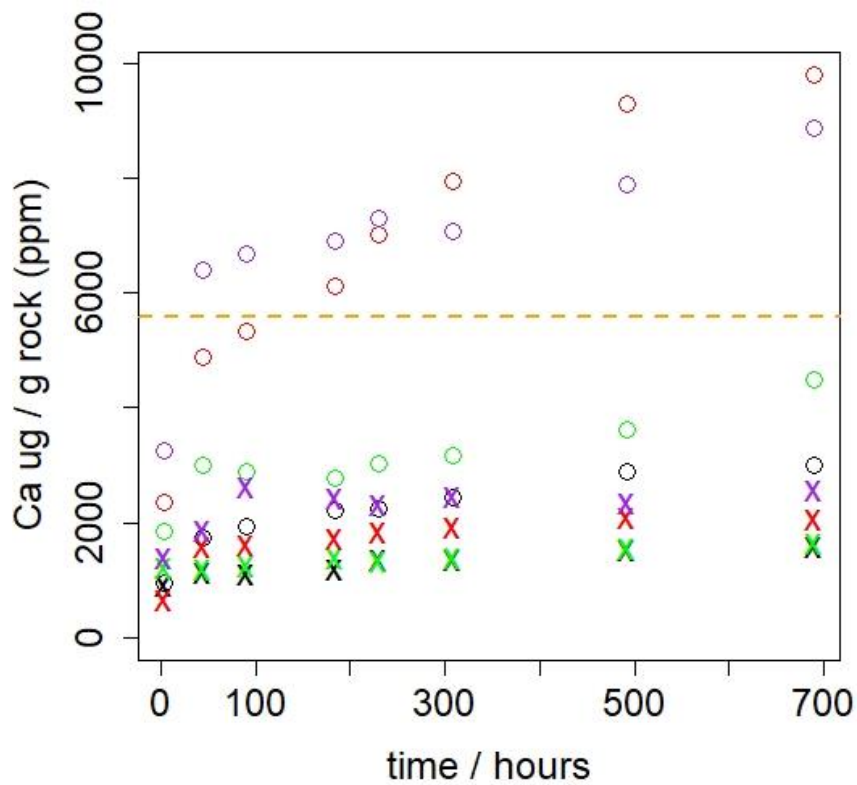
337 Fig. 4 – Arsenic concentrations are only above c. 1 µg/L in solutions with low (< 100 µg/L) Fe.

338 *4.1 Comparison of experimental and natural water chemistry*

339 A strong increase in the concentration of dissolved metals has been noted in previous studies of the
 340 effects of CO₂ in sandstones, and has been attributed to the dissolution of carbonates (e.g. Kjöllér et
 341 al. 2011; Rosenbauer et al. 2005; Shiraki and Dunn 2000; Varadharajan et al. 2013), or desorption
 342 mechanisms (e.g. Cahill et al. 2013; Mickler et al. 2013; Varadharajan et al. 2013; Weibel et al.,
 343 2014). Slower releases of elements, e.g. Fe, K and Al are then attributed to silicate or oxide
 344 dissolution by these authors. For the experiments reported here, a strong case can only be made for
 345 Pb and Zn mobilisation by the added CO₂, in that for these elements the median experimental
 346 concentrations substantially exceed the EEMS data (Pb median 30 µg/L with CO₂; EEMS 0.5 µg/L; Zn
 347 median 130 µg/L with CO₂; EEMS 9 µg/L), and the element concentrations in the CO₂ experiments
 348 exceed those of the controls (Pb 2 µg/L without CO₂; Zn 25 µg/L without CO₂).

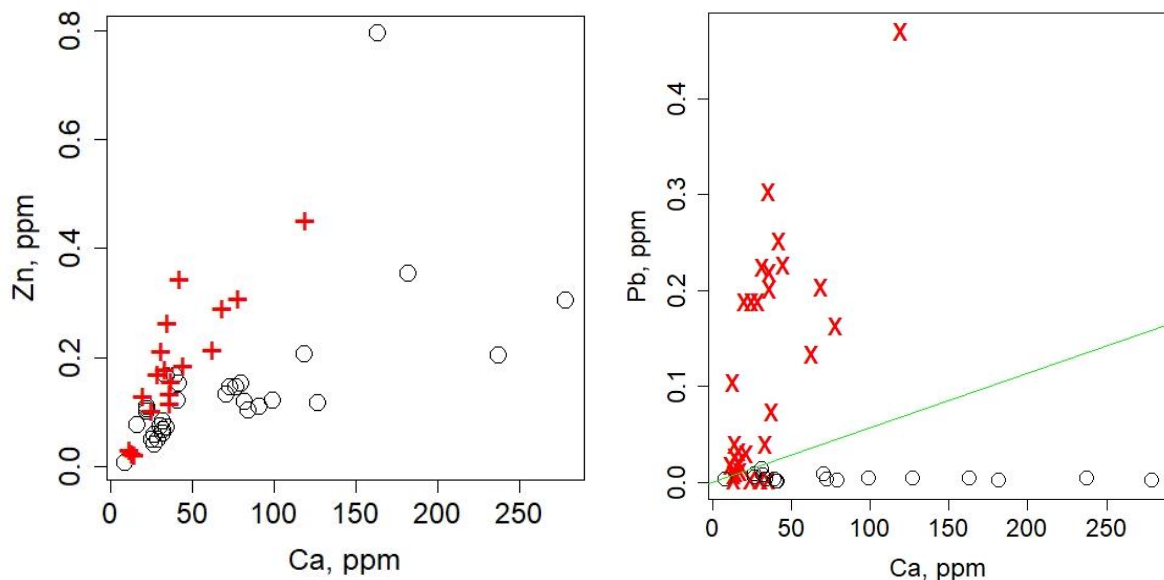
349

350 There is a strong 1:1 correlation between (Ca + Mg) and total alkalinity for both control and CO₂
 351 flasks, and Ba, Ca, Fe, Mg, Mn, and Sr exhibit, in virtually all cases, enhanced concentrations with the
 352 addition of CO₂ (Table 4A). This suggests that these elements are derived by the dissolution of
 353 calcite, as the only carbonate phase detected by XRD analysis (Table 3), driven by pH changes of
 354 approximately -1 pH unit. Note that for two of the leaching experiments with added CO₂, the
 355 calculated quantity of Ca released per g of rock exceeds that in the bulk analysis (Fig. 5), interpreted
 356 to be a product of the uneven distribution of calcite within the sandstone (Table 3). This may be
 357 partly a problem caused by limited sample size, constrained by the availability of core material from
 358 oilfield boreholes. While the quantity of sample required for analysis is small (approximately 1 g),
 359 using a sub-sample from a much larger sample (assuming effective homogenisation) might have
 360 reduced the discrepancy by incorporating more crystals of calcite in the experimental procedures.



361

362 Fig. 5 – Calculated mass of calcium released during the leaching experiments. Note the reaction
 363 appears to be ongoing for at least 2 of the flasks at the end of the experiments (red and purple
 364 circles: sample SA10 with CO₂). The orange dotted line is the whole-rock total Ca for sample SA7.



365

366 Fig 6A (left). Zn versus Ca in the leaching experiments show different ratios for samples SA7 (red
 367 crosses) and SA10 (black circles), for both +CO₂ and -CO₂ flasks (not differentiated).

368 Fig. 6B (right) - Pb versus Ca shows 2 trends, neither lies close to the ratio of Pb : Ca from the
 369 carbonate stage of the selective extraction procedure (green line).

370

371 Of the elements mobilised by the CO₂, Zn correlates weakly overall with Ca (Fig. 6A), however rock
372 samples SA7 and SA10 form separate trends. Zn could hence be interpreted to be released by the
373 dissolution of calcite with differing Zn contents in the 2 samples, higher for SA7. However, the
374 carbonate phase of the selective extraction procedure did not liberate Zn in detectable quantities,
375 and the quantity of Zn leached is a very high proportion of that present in the whole rock (c. 25 – 80
376 %; Table 5). Hence, if the Zn were derived by the dissolution of calcite, then almost all of the calcite
377 would have to be dissolved. The calculated dissolved mass of Ca however, ranges from c. 1 – 10 µg /
378 g rock, a small proportion of the c. 2900 ppm determined in the carbonate stage of the selective
379 extraction procedure (Table 6). An alternative explanation of the correlation of Zn with Ca is that it
380 reflects a common control, possibly pH change or time for slow desorption and dissolution reactions.
381 Given that the mean mass of Zn leached per g of rock is close to the total in the bulk rock analysis,
382 the preferred explanation is that the Zn is present in the sandstones absorbed onto mineral (Fe, Mn
383 and Al oxides or hydroxides, clay minerals; Lions et al., 2014) or organic surfaces, and is hence
384 released almost entirely during the leaching experiments.

385

386 The same patterns and arguments apply to Pb (Fig. 6B) which for sample SA7 would require in excess
387 10 % of the total calcite to be dissolved if it were to be obtained from this source, i.e. far in excess of
388 the quantity dissolved as inferred from the measured Ca concentrations. As an alternative source, Pb
389 is typically present in K-feldspars in the range of 10 – 1000 ppm (Smith and Brown, 1988), though for
390 sample SA7 the Pb concentrations (relative to K) would require dissolution of a feldspar with > 1 %
391 Pb, which is unfeasible, or for much of the liberated K to be precipitated as, for example, a K-rich
392 clay mineral such as illite. For SA10, which has much lower concentrations of Pb compared to K
393 (median 30 and 70000 µg/L with CO₂, respectively), there is no correlation between the two
394 elements. This either indicates that the dissolution of K-feldspar is not the source of the Pb, or that
395 the individual feldspar crystals have varying Pb contents and reactivities. Interestingly, modelling
396 using Phreeqc indicates an equilibrium K concentration of c. 30,000 µg / L in the presence of K-
397 feldspar and quartz under the experimental conditions, which is the upper boundary of observed K
398 concentrations, possibly implying an approach to equilibrium with K-feldspar for sample SA10. It is
399 hence difficult to quantify the contribution of K-feldspar dissolution to the Pb budget for sample
400 SA10, though a contribution certainly cannot be excluded. The contribution of plagioclase
401 dissolution is even more difficult to quantify, as all the major elements contributed by plagioclase
402 are also sourced from carbonates (Ca), other aluminosilicates (Si, Al) or dissolved in porewater in
403 concentrations that substantially exceed any likely contribution from plagioclase (Na). Hence, from
404 the above discussion, Pb is also interpreted to be desorbed from mineral (clay minerals; Fe-oxides)
405 and / or organic matter surfaces with the possible exception of the Pb in sample SA10 which could
406 be sourced from K-feldspars. Given that both Pb and Zn are sourced by desorption, this would make
407 for difficult prediction of likely mobilisation during CO₂ injection, as the measurement of absorbed
408 Pb and Zn on mineral surfaces will not be simple. Neither the selective extraction procedure nor the
409 whole rock analysis appears to provide useful information in this context and are not viable
410 alternatives to the leaching experiments. Indeed, the simplest method for the determination of trace
411 metal will most likely be desorption under simulated reservoir conditions, as with the leaching
412 experiments reported here.

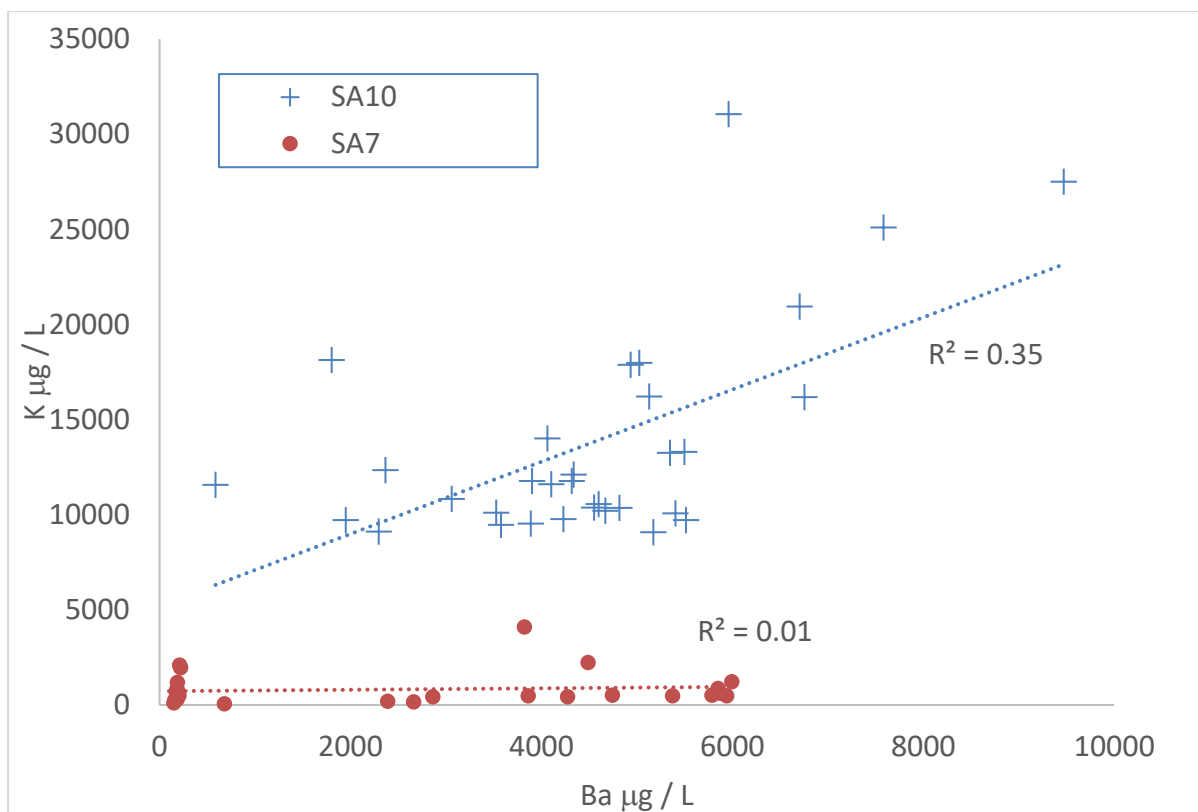
413 Lions et al. (2014) noted that, for both Pb and Zn, dissolution experiments conducted in a laboratory
414 setting (e.g. Little and Jackson, 2010; Lu et al., 2010) show significantly higher degrees of
415 mobilisation than in-situ experiments (Kharaka et al., 2010; Trautz et al., 2013; Cahill and Jakobsen,
416 2013). It has hence been suggested that, in natural systems, scavenging of mobilised metals along
417 fluid flow paths reduces Pb and Zn concentrations, which are artificially intensified under laboratory
418 conditions (Lions et al., 2014). It is therefore concluded that the relatively high Pb and Zn
419 concentrations in the experiments reported here are unlikely to be found in a subsurface injection
420 scenario. Hence, if porewater from the Captain Sandstone Member were to be produced to the
421 surface and disposed of by over-boarding into the North Sea, then the trace element load of the
422 waters will be comparable to existing practise during hydrocarbon operations, and experimental
423 tests such as those presented here would represent overestimates of the potential for metal
424 pollution.

425

426 *4.2 Limitations of the experimental method*

427

428 Because the rock samples utilised in the experiments reported here are from oilfield core, they have
429 been potentially contaminated by the 'mud' used in drilling, an issue that has long been known to
430 make difficult the extraction of uncontaminated porewaters from core samples e.g. Lovelock et al.
431 (1975). Such mud contains barite (North, 1985) and for borehole 13/24a-4 had KCl contents of c. 60
432 mg / L at the relevant depth of drilling (unpublished End of Well Report by Haliburton for BG
433 Exploration and Production, 1998). There is a correlation between K and Ba for sample SA10 which is
434 significant for 95 % confidence (Fig. 7; $R^2 = 0.35$, $n = 32$) but not for SA7 ($R^2 = 0.01$, $n = 28$). The range
435 of concentrations for the 2 samples used is similar for Ba, but significantly different for K (Fig. 7).
436 Modelling a solution in equilibrium with barite using Phreeqc gives a concentration of c. 2400 $\mu\text{g} / \text{L}$
437 under the conditions of the experiments. As many of the Ba concentrations exceed the modelled
438 value, and there is no clustering around the value, it is concluded that barite is not buffering Ba, nor
439 even an significant source of the element in the experiments. For K, simple mass balance shows that
440 the experimental concentrations massively exceed those that could be produced even if the
441 porefluids within the sandstone were fully replaced by drilling mud, and this were evaporated to
442 dryness during sample storage, and then fully re-dissolved in the experimental brine (calculated at c.
443 50 $\mu\text{g} / \text{L}$). Phreeqc modelling indicates an equilibrium concentration of K of c. 30,000 $\mu\text{g} / \text{L}$ in the
444 presence of K-feldspar and quartz, which is the upper boundary of observed concentrations, possibly
445 implying an approach to equilibrium during the experiments for sample SA10. Sample SA7 has much
446 lower concentrations, so that either K-feldspar is absent (and the K comes from another source), or
447 any present is less reactive due to for example, a much lower surface area. Either way, there is no
448 evidence to support significant contamination of the samples by drilling mud.



449

450 Fig. 7 – Possible indicators of rock sample contamination by drilling mud. There is no strong
 451 relationship between K and Ba. The range of concentrations for the 2 samples (SA7 in red, SA10 in
 452 black) is similar for Ba, but significantly different for K.

453 The experiments here were conducted in open flasks, which though flushed with CO₂ were in
 454 contact with the atmosphere through the condenser, as were the reagents prior to the start of the
 455 experiments. The redox conditions will hence differ from those likely to be found in the subsurface,
 456 although the oxygen partial pressure was most likely substantially below that of the atmosphere for
 457 much of the duration of the experiments. The duration of the experiments was very short compared
 458 to the hoped-for residence time of CO₂ in engineered storage (10,000 years) or even the lifetime of a
 459 typical CO₂ injection facility (30 – 50 years?). Longer experiments are logistically more difficult.
 460 However, calculated trace metal loads are either stable or falling by the end of the experiments (Fig.
 461 3), so there is no evidence that running the experiments for longer would materially alter the
 462 conclusions of the work.

463

464 In the experiments reported here, the initial porewater were not in equilibrium with the mineral
 465 phases in the rock samples. Hence, some initial reaction between brine and host rock would be
 466 expected; this would not be due to the presence of the CO₂. Here, control experiments were ran
 467 without added CO₂, so that any reactions due to this disequilibrium will be common to both control
 468 and CO₂ flasks. For this reason, the leaching of Cu is interpreted to be due to the establishment of
 469 initial equilibrium, as concentrations are similar for control and CO₂ flasks (median 90 µg/L without
 470 CO₂; 100 µg/L with CO₂), despite both being higher than the EEMS data (median 0.8 µg/L). Other
 471 authors have run parallel experiments with an inert gas (N₂) as a control (e.g. Weibel et al., 2014) or

472 attempted to recreate the chemistry of the in-situ brine as closely as practicable (e.g. Fisher et al.,
473 2010). An alternative approach, to leave the experiments to reach equilibrium before adding the
474 CO₂, has not been attempted most likely due to the excessive time required, or the difficulty of
475 establishing that equilibrium has been established.

476

477 All of the experiments reported in the literature, including those reported here, are run under
478 conditions in which bacteria or other micro-organisms can survive. There is no evidence of biological
479 activity in the experiments, but neither is there proof that such activity did not take place. The role
480 of micro-organisms in subsurface reactions has long been recognised, most commonly in mudrocks
481 (e.g. Irwin et al., 1977) and more controversially in sandstones (e.g. Folk and Lynch, 1997). The
482 possibility of interference of micro-organisms in the experiments cannot hence be eliminated. A
483 biocide could possibly have been added to the experiments to prevent this.

484

485 The results from the two rock samples used (SA7 and SA10) are significantly different for Cu (40 vs
486 150 µg/L respectively) and Pb (200 µg/L vs BDL), as well as for the total Ca dissolved in the +CO₂
487 experiments (35000 vs 85000 µg/L; Fig. 6). The results of the leaching experiments therefore agree
488 with the XRD analysis: sample SA10 has more calcite (1.6 ± 0.4 % XRD) than sample SA7 (0.37 ± 0.06 ,
489 XRD). Given that calcite is typically present in deeply buried sandstones as unevenly distributed
490 single crystals, this is not surprising. As the differences are not due to sample contamination by
491 drilling mud, they demonstrate natural sample heterogeneity, a feature of sandstones.
492 Consequently, a leaching experiment based upon a single rock sample, even if replicated, cannot
493 capture natural variation within a reservoir. To fully characterise the likely trace metal load of any
494 produced waters would require a representative number of rock samples, presumably spread
495 throughout the reservoir of interest, to capture the inevitable natural heterogeneity.

496 The analytical limit of detection (LoD) for 7 of the 8 trace metals is less than the predicted no-effect
497 concentrations (PNEC; Table 2). The exception is Cu, where the LoD (2.9 µg / L) exceeds the PNEC
498 value (2.6 µg / L). As the two values differ by only c. 10%, this is not considered to influence the
499 conclusions of this study. It is also noted that the concentrations of Cu in both the CO₂ and no-CO₂
500 experiments (median 100 µg/L with CO₂; 90 µg/L without CO₂) substantially exceed the LoD and
501 PNEC values (2.9 and 2.6 µg / L respectively; Table 2), and that although the experimental Cu
502 concentrations substantially exceed that of the Captain Sandstone data from the EEMS database
503 (median 0.8 µg/L), there is no evidence that the CO₂ enhances the leaching.

504

505 **5. Conclusions**

506 Batch experiments using samples of the Captain Sandstone Member suggest that the mobility of 8
507 potentially toxic trace metals is low in the presence of high concentrations of CO₂. The
508 concentrations of these metals leached from sandstones are often lower than analytical detection
509 limits, which are (for 7 of the 8 trace metals considered) lower than concentrations recommended
510 by the OSPAR commission for produced water discharges from offshore installations. Where analysis

511 was possible, the concentrations generally are similar to those of natural brine from the Captain
512 Sandstone Member, suggesting minimal extra trace metal load compared to existing hydrocarbon
513 operations.

514 For As, Cd, Cr, Hg, and Pb, the experiments have effectively recreated trace metal load of the native
515 porewaters of the Captain Sandstone aquifer despite the difference in pressure, redox and timescale
516 of the experiments compared to in-situ subsurface conditions. The use of rock chips versus
517 disaggregated grains made little difference to the results, the only elements that show any apparent
518 difference are those for which the majority of analyses were below the limit of detection (As, Cd) so
519 that a meaningful interpretation cannot be made. Arsenic concentrations notably decreased in the
520 presence of CO₂, probably due to increased absorption onto Fe-oxides under lowered pH conditions.

521 Only Pb and Zn were convincingly mobilised during the CO₂ – rich experiments mobilised (median 30
522 vs 2 µg/L for Pb; 130 vs 25 µg/L for Zn), and are interpreted to have been desorbed from mineral or
523 organic matter surfaces, although the contribution from the dissolution of feldspars is difficult to
524 quantify. Both Pb and Zn have been previously reported to be more easily mobilised in experiments
525 than during in-situ CO₂ injection, due to re-absorption onto mineral surfaces. It is hence considered
526 that the production of native porewater from the Captain Sandstone Member, for pressure control
527 during the injection of CO₂, is unlikely to produce a higher load of trace metals than existing oil and
528 gas production from the same reservoir.

529 The results from the two rock samples used are significantly different for Cu (median 40 vs 150 µg/L)
530 and Pb (median 200 µg/L vs BDL), although they are from the same reservoir sandstone.
531 Consequently, a representative number of samples would have to be used to determine potential
532 reaction with a high degree of confidence.

533 Neither the whole-rock analysis nor the selective extraction procedure (either of which could have
534 provided quicker and cheaper alternatives to the leaching experiment) provided useful information
535 about the leached trace metal loads. Consequently, the leaching experiments appear to be the only
536 practical way to assess trace metal loading.

537

538 **Acknowledgements**

539

540 KC was co-funded by the UK EPSRC and ScottishPower. Neither organisation was involved in the
541 design or interpretation of the work. We thank Walter Geibert for assisting in the ICP-OES analysis.
542 We thank the British Geological Survey for the core samples. Two reviewers contributed to the
543 clarity and accuracy of the manuscript.

544

545 **References:**

546

547 Allen, M.J., Faulkner, D.R., Worden, R.H., Rice-Birchall, E., Katirtsidis, N., and Utley, J.E.P., 2020.
548 Geomechanical and petrographic assessment of a CO₂ storage site: Application to the Acorn CO₂
549 Storage Site, offshore United Kingdom. *International Journal of Greenhouse Gas Control* 94, 102923.

550 Boiteau, R. M., Till, C. P., Ruacho, A., Bundy, R. M., Hawco, N. J., McKenna, A. M., Barbeau, K. A.,
551 Bruland, K. W., Saito, M. A., & Repeta, D. J., 2016. Structural Characterization of Natural Nickel and
552 Copper Binding Ligands along the US GEOTRACES Eastern Pacific Zonal Transect. *Frontiers in Marine*
553 *Science* 3, 1-16. doi:10.3389/fmars.2016.00243

554 Bowman, K. L., Hammerschmidt, C. R., Lamborg, C. H., & Swarr, G., 2015. Mercury in the North
555 Atlantic Ocean: The U.S. GEOTRACES zonal and meridional sections. *Deep Sea Research Part II:*
556 *Topical Studies in Oceanography* 116, 251–261. doi:10.1016/j.dsr2.2014.07.004

557 Cahill, A. G. and Jakobsen, R., 2013. Hydro-geochemical impact of CO₂ leakage from geological
558 storage on shallow potable aquifers: A field scale pilot experiment. *International Journal of*
559 *Greenhouse Gas Control* 19, 678–688.

560 Cahill, A. G., Jakobsen, R., Mathiesen, T. B., and Jensen, C. K., 2013. Risks attributable to water
561 quality changes in shallow potable aquifers from geological carbon sequestration leakage into
562 sediments of variable carbonate content. *International Journal of Greenhouse Gas Control* 19, 117–
563 125.

564 Cutter, G.A., L.S. Cutter, and A.M. Featherstone, 2001. Antimony and arsenic biogeochemistry in the
565 western Atlantic Ocean. *Deep-Sea Research*, 48:2895-2915.

566 Fischer, S., Liebscher, A., and Wandrey, M., 2010. CO₂–brine–rock interaction — First results of
567 longterm exposure experiments at in situ P–T conditions of the Ketzin CO₂ reservoir. *Chemie der*
568 *Erde - Geochemistry* 70, 155–164.

569 Folk, R.L. (1974) *Petrology of sedimentary rocks*, 170 pp. Austin. Texas, Hemphill Publication
570 Company.

571 Folk, R.L., and Lynch, F.L., 1997. The possible role of nanobacteria (dwarf bacteria) in clay-mineral
572 diagenesis and the importance of careful sample preparation in high-magnification SEM study.
573 *Journal of Sedimentary Research* 67, 583-589.

574 Hsia, T-H, Lo, S.-L., Lin, C.-F. and Lee, D.-Y., 1994. Characterization of arsenate adsorption on hydrous
575 iron oxide using chemical and physical methods. *Colloids and Surfaces A: Physicochemical and*
576 *Engineering Aspects* 85, 1-7.

577 Irwin, H., Curtis, C., and Coleman, M., 1977. Isotopic evidence for source of diagenetic carbonate
578 formed during burial of organic-rich sediments. *Nature*, 269, 209-213.

579 Jeandel, C., and Minster, J. F., 1987. Chromium behavior in the ocean: global versus regional
580 processes. *Global Biogeochemical Cycles* 1, 131-154.

581 Kirsch, K., Navarre-Sitchler, A. K., Wunsch, A., and McCray, J. E., 2014. Metal release from
582 sandstones under experimentally and numerically simulated CO₂ leakage conditions. *Environmental*
583 *Science & Technology* 48, 1436–1442.

584 Kjölller, C., Weibel, R., Bateman, K., Laier, T., Nielsen, L. H., Frykman, P., and Springer, N., 2011.
585 Geochemical impacts of CO₂ storage in saline aquifers with various mineralogy - Results from
586 laboratory experiments and reactive geochemical modeling. *Energy Procedia* 4, 4724–4731.

587 Kharaka, Y. K., Thordsen, J. J., Kakouros, E., Ambats, G., Herkelrath, W. N., Beers, S. R., Birkholzer, J.
588 T., Apps, J., Spycher, N. F., Zheng, L., Trautz, R. C., Rauch, H.W., and Gullickson, K. S., 2010. Changes
589 in the chemistry of shallow groundwater related to the 2008 injection of CO₂ at the ZERT field site,
590 Bozeman, Montana. *Environmental Earth Sciences* 60, 273–284.

591 Lions, J., Devau, N., De Lary, L., Dupraz, S., Parmentier, M., Gombert, P., and Dictor, M. C., 2014.
592 Potential impacts of leakage from CO₂ geological storage on geochemical processes controlling fresh
593 groundwater quality: a review. *International Journal of Greenhouse Gas Control* 22, 165–175.

594 Little, M. G.; Jackson, R. B., 2010. Potential impacts of leakage from deep CO₂ geosequestration on
595 overlying freshwater aquifers. *Environ. Sci. Technol.* 44, 9225 – 9232.

596 Lovelock, P. E. R., Price, M., Tate, T. K., J., 1975. *Inst. Water Eng.*, 29, 157-74.

597 Lu, J., Mickler, P. J., Nicot, J.-P., Yang, C., and Romanak, K. D., 2014. Geochemical impact of oxygen
598 on siliciclastic carbon storage reservoirs. *International Journal of Greenhouse Gas Control* 21, 214–
599 231.

600 Lu, J., Partin, J. W., Hovorka, S. D., and Wong, C., 2010. Potential risks to freshwater resources as a
601 result of leakage from CO₂ geological storage: a batch-reaction experiment. *Environmental Earth*
602 *Sciences* 60, 335–348.

603 Melvin, K., Cummine, C., Youles, J. and Williams, H.L., Graham, G.M. and Dyer, S.J., 2008. Optimising
604 calcium naphthenate control in the Blake Field. *Society of Petroleum Engineers* 114123.

605 Mickler, P. J., Yang, C., Scanlon, B. R., Reedy, R., and Lu, J., 2013. Potential impacts of CO₂ leakage on
606 groundwater chemistry from laboratory batch experiments and field push-pull tests. *Environmental*
607 *Science and Technology* 47, 10694–10702.

608 Middag, R., van Heuven, S. M. A. C., Bruland, K. W., & de Baar, H. J. W., 2018. The relationship
609 between cadmium and phosphate in the Atlantic Ocean unravelled. *Earth and Planetary Science*
610 *Letters* 492, 79–88. doi:10.1016/J.EPSL.2018.03.046

611 North, F.K., 1985, *Petroleum Geology*. Allen and Unwin, London.

612 OSPAR Commission (2014). Establishment of a list of Predicted No Effect Concentrations (PNECs) for
613 naturally occurring substances in produced water (OSPAR Agreement 2014-05).
614 [https://assets.publishing.service.gov.uk/government/uploads/system/uploads/attachment_data/file](https://assets.publishing.service.gov.uk/government/uploads/system/uploads/attachment_data/file/361476/OSPAR_RBA_Predicted_No_Effect_Concentrations_PNECs_Background_Document.pdf)
615 [/361476/OSPAR_RBA_Predicted_No_Effect_Concentrations_PNECs_Background_Document.pdf](https://assets.publishing.service.gov.uk/government/uploads/system/uploads/attachment_data/file/361476/OSPAR_RBA_Predicted_No_Effect_Concentrations_PNECs_Background_Document.pdf)
616 Accessed 18.5.2020.

617 Pale Blue Dot Energy, 2016. Progressing Development of the UK's Strategic Carbon Dioxide Storage
618 Resource. [https://pale-blu.com/2016/04/25/progressing-development-of-the-uks-strategic-carbon-](https://pale-blu.com/2016/04/25/progressing-development-of-the-uks-strategic-carbon-dioxide-storage-resource/)
619 [dioxide-storage-resource/](https://pale-blu.com/2016/04/25/progressing-development-of-the-uks-strategic-carbon-dioxide-storage-resource/)
620

- 621 Pinnock, S. J., Clitheroe, A. R. J. and Rose, P. T. S., 2003. The Captain Field, Block 13/22a, UK North
622 Sea. In: Geological Society, London, Memoir 20, 431-441.
- 623 Rosenbauer, R. J., Koksalan, T., and Palandri, J. L., 2005. Experimental investigation of CO₂-brine-rock
624 interactions at elevated temperature and pressure: Implications for CO₂ sequestration in deep-saline
625 aquifers. *Fuel Processing Technology* 86, 1581–1597.
- 626
627 SCCS, 2011, Progressing Scotland's CO₂ storage opportunities.
628 <http://www.geos.ed.ac.uk/sccs/progress-to-co2-storage-scotland/ProgressingScotlandCO2Opps.pdf>
- 629 Schlitzer, R. and 286 others, 2018. The GEOTRACES Intermediate Data Product 2017. *Chemical*
630 *Geology* 493, 210–223. doi:10.1016/j.chemgeo.2018.05.040
- 631 Shiraki, R. and Dunn, T. L., 2000. Experimental study on water-rock interactions during CO₂ flooding
632 in the Tensleep Formation, Wyoming, USA. *Applied Geochemistry* 15, 265–279.
- 633 Smith, J.V. and Brown, W.L., 1988. Feldspar Minerals, Volume 1, Crystal structures, physical,
634 chemical and microtextural properties. Springer-Verlag, Berlin.
- 635 Tessier, A., Campbell, P. G. C., & Bisson, M., 1979. Sequential Extraction Procedure for the Speciation
636 of Particulate Trace Metals. *Analytical Chemistry* 51:844–851.
- 637 Trautz, R. C., Pugh, J. D., Varadharajan, C., Zheng, L., Bianchi, M., Nico, P. S., Spycher, N. F., Newell, D.
638 L., Esposito, R. A., Wu, Y., Dafflon, B., Hubbard, S. S., and Birkholzer, J. T., 2013. Effect of Dissolved
639 CO₂ on a Shallow Groundwater System: A Controlled Release Field Experiment. *Environmental*
640 *Science & Technology* 47, 298-305.
- 641 Vandecasteele, C. and Block, C. B., 1993. Modern Methods for Trace Element Determination. John
642 Wiley & Sons Ltd., Chichester.
- 643 Varadharajan, C., Tinnacher, R. M., Pugh, J. D., Trautz, R. C., Zheng, L., Spycher, N. F., Birkholzer, J. T.,
644 Castillo-Michel, H., Esposito, R., and Nico, P. S., 2013. A laboratory study of the initial effects of
645 dissolved carbon dioxide (CO₂) on metal release from shallow sediments. *International Journal of*
646 *Greenhouse Gas Control* 19, 183–211.
- 647 Weibel R., Kjølner, C., Bateman, K., Laier, T., Nielsen, L.H., Purser, G., 2014. Carbonate dissolution in
648 Mesozoic sand- and claystones as a response to CO₂ exposure at 70°C and 20 MPa. *Applied*
649 *Geochemistry* 42, 1–15.
- 650 Wigley, M., Kampman, N., Chapman, H. J., Dubacq, B., & Bickle, M. J., 2013. In situ redeposition of
651 trace metals mobilized by CO₂-charged brines. *Geochemistry, Geophysics, Geosystems* 14, 1321–
652 1332. <http://doi.org/10.1002/ggge.20104>
- 653 Wyatt, N. J., Milne, A., Woodward, E. M. S., Rees, A. P., Browning, T. J., Bouman, H. A., Worsfold, P.
654 J., & Lohan, M. C., 2014. Biogeochemical cycling of dissolved zinc along the GEOTRACES South
655 Atlantic transect GA10 at 40°S. *Global Biogeochemical Cycles* 28, 44–56. doi:10.1002/2013GB004637
- 656
657

658 Zheng, L. and Spycher, N., 2018. Modeling the potential impacts of CO₂ sequestration on shallow
659 groundwater: The fate of trace metals and organic compounds before and after leakage stops.
660 Greenhouse Gas Sci Technol. 8, 161–184. DOI: 10.1002/ghg

661

662 Table 4A. Porewater composition of the batch experiments with added CO₂. No blank correction except for Hg (blank experiments excepted).

663

Flask	Type	Bubbled CO ₂	Date	Days	Hours	pH	HCO ₃ ⁻ mg/L	CO ₃ ²⁻ mg/L	Al μg/L	As μg/L	Ba μg/L	Ca μg/L	Cd μg/L	Cr μg/L	Cu μg/L	Fe μg/L	Hg μg/L	K μg/L	Mg μg/L	Mn μg/L	Na μg/L	Ni μg/L	Pb μg/L	Ti μg/L	U μg/L	V μg/L	Zn μg/L	
F1	Blank	Y	31/05/2011	1	4	4.66	65	30	14.02	0	6.04	1750	0.0046	0	54.37	178.07	2.22	445.13	37.96	1.42	0	0	0	0	0	1.95	5.6	
F1	Blank	Y	01/06/2011	2	16	4.30	50	25																				
F1	Blank	Y	02/06/2011	3	45	4.45	25	10	175.81	0	9.63	1640	0.21	0.46	91.51	14.18	5.63	358.02	36.58	1.26	0	0	3.58	0		1.49	0	
F1	Blank	Y	03/06/2011	4	69.5	4.77	50	25																				
F1	Blank	Y	04/06/2011	5	91	4.73	30	15	5.02	0	8.34	390	0.43	0	157.77	118.3	3.96	323.34	20.31	2.55	0	15.48	0	0	0	1.52	61.24	
F1	Blank	Y	05/06/2011	6	109.5	5.36	65	30																				
F1	Blank	Y	06/06/2011	7	137	4.60	55	25																				
F1	Blank	Y	08/06/2011	9	183.5	4.51	50	25	148.39	1.67	0	1830	0	0	66.01	0	2.34	87.86	0	0	876.49	54.88	0	0	0	0	0	0
F1	Blank	Y	09/06/2011	10	210.5	4.06																						
F1	Blank	Y	10/06/2011	11	229.5	4.27	45	20	70.95	0	2.47	1140	0	0	103.98	0	2.26	291.72	0	0	756.13	3.09	13.22	0	0	0	0	0
F1	Blank	Y	12/06/2011	13	285	3.96																						
F1	Blank	Y	13/06/2011	14	308	3.90	55	25	226.03	0	5.09	1630	0	0.18	102.67	34.56	2.22	146.59	23.46	0	1635.37	5.16	2.79	0	0	0	0	0
F1	Blank	Y	15/06/2011	16	349.5	3.91																						
F1	Blank	Y	21/06/2011	22	491.5	5.01	55	30	5.02	0	0	0	0	0.87	147.9	35.97	1.84	1187.48	83.86	0	4650.49	0	4.06	0	0	0	0	0
F1	Blank	Y	29/06/2011	30	689.5	4.95	50	25	203.86	0	11.49	1600	0	0.66	83.6	48.76	1.85	1526.74	19.97	1.05	8504.05	0.19	6.26	6.56	0	0	0	0
F2	SA7_Chip	Y	31/05/2011	1	4	4.79	50	25	0	0	679.81	11030	0.2554	1.3002	12.77	0	0	57.12	151.05	24.83	0	9.9794	104.3051	0	0	0	0	19.1
F2	SA7_Chip	Y	01/06/2011	2	16	5.03	80	40																				
F2	SA7_Chip	Y	02/06/2011	3	45	6.20	105	50	0	0	2389.41	23370	0.15	0	13.43	433.02	0	189.11	288.19	106.96	0	10.8294	185.3	0	0	0.43	101.73	
F2	SA7_Chip	Y	03/06/2011	4	69.5	6.23	105	50																				
F2	SA7_Chip	Y	04/06/2011	5	91	6.11	105	50	14.38	0	2861.94	28350	0	3.4202	7.71	0	0	424.73	387.28	132.72	0	1.23	188.4351	0	0	0.19	108.22	
F2	SA7_Chip	Y	05/06/2011	6	109.5	6.46	120	60																				
F2	SA7_Chip	Y	06/06/2011	7	137	6.46	120	60																				
F2	SA7_Chip	Y	08/06/2011	9	183.5	6.12	120	60	0	0	3861.34	34160	0	1.0002	67.55	34.075	0	475.59	617.997	199.5843	0	0	201.6351	0	0	0	115.07	
F2	SA7_Chip	Y	09/06/2011	10	210.5	6.10																						
F2	SA7_Chip	Y	10/06/2011	11	229.5	6.40	135	65	0	0	4273.37	35150	0	0.5702	42.25	110.385	0	435.34	649.417	227.3943	0	8.85	206.28	0	0	0	132.09	
F2	SA7_Chip	Y	12/06/2011	13	285	5.99																						
F2	SA7_Chip	Y	13/06/2011	14	308	6.12	160	80	0	0	4741.99	43170	0	0.63	33.74	283.88	0	513.76	793.36	281.0443	0	10.09	223.85	0	0	0	184.66	
F2	SA7_Chip	Y	15/06/2011	16	349.5	6.18																						
F2	SA7_Chip	Y	21/06/2011	22	491.5	6.99	185	90	0	0	5993.14	68331	0	0	61.61	0	0	1223.8	1410.03	539.5143	0	22.1094	200.14	12.31	0	0	288.29	
F2	SA7_Chip	Y	29/06/2011	30	689.5	7.43	235	115	0	0	5849.43	76530	0	0	86.29	263.97	0	870.26	1847.45	683.98	0	24.31	157.04	0	0	0	306.04	
F3	SA7_Grain	Y	31/05/2011	1	4	5.19	105	50	0	4.285	2660.24	18410	0.2654	1.5902	26.11	0	0	170.13	179.3	59.41	0	3.4994	189.1651	0	0	0	124.04	
F3	SA7_Grain	Y	01/06/2011	2	16	5.65	115	55																				
F3	SA7_Grain	Y	02/06/2011	3	45	6.39	100	50	0	0	5941.05	33450	0	0	82.93	922.62	0	482.87	357.22	187.91	0	3.5694	299.56	0	0	2.36	262.99	
F3	SA7_Grain	Y	03/06/2011	4	69.5	6.66	150	75																				
F3	SA7_Grain	Y	04/06/2011	5	91	6.92	95	45	137.92	0	5785.26	32780	0	3.9502	0	0	0	515.51	493.16	136.25	0	0.43	39.5951	0	0	0.35	116.99	
F3	SA7_Grain	Y	05/06/2011	6	109.5	7.34	115	55																				
F3	SA7_Grain	Y	06/06/2011	7	137	8.20	115	55																				
F3	SA7_Grain	Y	08/06/2011	9	183.5	6.09	125	60	0	0	5872.78	29480	0	1.5002	145.13	53.025	0	611.66	627.587	185.9843	0	0	225.0951	0	0	0	209.95	
F3	SA7_Grain	Y	09/06/2011	10	210.5	5.90																						
F3	SA7_Grain	Y	10/06/2011	11	229.5	6.75	120	60	0	0	5372.93	35890	0	0	34.72	0	0	487.76	639.007	197.9143	0	376.35	60.63	0	0	0	154.04	

668 Table 4B. Porewater composition from the batch experiments with no added CO₂. No blank correction except for Hg (blank experiments excepted)..

Flask	Type	Bubbled CO ₂	Date	Days	Hours	pH	HCO ₃ ⁻ mg/L	CO ₃ ²⁻ mg/L	Al μg/L	As μg/L	Ba μg/L	Ca μg/L	Cd μg/L	Cr μg/L	Cu μg/L	Fe μg/L	Hg μg/L	K μg/L	Mg μg/L	Mn μg/L	Na μg/L	Ni μg/L	Pb μg/L	Ti μg/L	U μg/L	V μg/L	Zn μg/L
B1	Blank	N	31/05/2011	1	4	6.41	55	30	49.41	2.01	11.42	2990	0.71	4.23	55.18	68.63	46858.8	1007.96	224.81	11.55	119.01	0.0406	1.84	10.84	0	1.52	28.7
B1	Blank	N	01/06/2011	2	16	6.67	65	30																			
B1	Blank	N	02/06/2011	3	45	6.57	70	35	0	0	1.79	0	0.16	0.51	76.01	0	13.99	641.17	10.33	1.6	119.01	0.0406	0	0	0	1.36	1.8
B1	Blank	N	03/06/2011	4	69.5	8.26	60	30																			
B1	Blank	N	04/06/2011	5	91	8.26	55	25	0	0	15.18	5270	0	0	93.51	0	6.25	320.69	8.08	0.0657	119.01	0.0406	0	0	0	1.49	7.57
B1	Blank	N	05/06/2011	6	109.5	6.95	55	25																			
B1	Blank	N	06/06/2011	7	137	7.04	20	10																			
B1	Blank	N	08/06/2011	9	183.5	4.77	40	20	196.78	3.97	0	1410	0	0.19	56.9	0	3.89	0	0	0	0	8.52	0	0	0	0	0
B1	Blank	N	09/06/2011	10	210.5	4.66																					
B1	Blank	N	10/06/2011	11	229.5	5.07	50	25	0	0	0	1170	0	2.05	46.98	0	2.72	0	0	0	0	2.12	0	4.55	0	0	0
B1	Blank	N	12/06/2011	13	285	5.35																					
B1	Blank	N	13/06/2011	14	308	5.10	45	20	70.18	0	0	470	0	0	27.17	0	2.97	0	0	0	0	271.12	0	0	0	0	0
B1	Blank	N	15/06/2011	16	349.5	4.80																					
B1	Blank	N	21/06/2011	22	491.5	4.76	55	25	0	0	0	250	0	0	117.4	4.38	4.89	702.17	1.143	0	2122.93	0	1.2	5.45	0	0	0
B1	Blank	N	29/06/2011	30	689.5	5.85	55	30	76.6	0	3.34	1180	0	2.38	78.64	14.67	3.19	892.91	83.23	1.7	2881.81	0	1.77	2.38	0	0	0
B2	SA7_Chip	N	31/05/2011	1	4	6.31	50	25	0	0	97.54	8660	0	0	43.9	60.71	0	0	0	7.07	0	0	16.16	0	0	0.14	2.53
B2	SA7_Chip	N	01/06/2011	2	16	6.91	35	15																			
B2	SA7_Chip	N	02/06/2011	3	45	6.68	45	20	0	0	155.76	14771	0	0.62	0	8.205	0	0	198.36	14.12	0	0	10.5951	0	0	0.76	0
B2	SA7_Chip	N	03/06/2011	4	69.5	7.45	45	20																			
B2	SA7_Chip	N	04/06/2011	5	91	7.37	75	40	0	0	149.94	9100	0.2654	1.6402	14.92	0	0	104.45	196.53	21.0643	0	0	26.4951	0	0	0.1	13.65
B2	SA7_Chip	N	05/06/2011	6	109.5	6.83	55	25																			
B2	SA7_Chip	N	06/06/2011	7	137	6.88	75	35																			
B2	SA7_Chip	N	08/06/2011	9	183.5	5.17	80	40	0	0	180.04	14980	0	0	15.79	0	0	374.4	463.367	28.2543	0	10.41	20.82	0	0	0	0
B2	SA7_Chip	N	09/06/2011	10	210.5	5.34																					
B2	SA7_Chip	N	10/06/2011	11	229.5	6.41	60	30	160.49	0	184.02	20310	0	0	48.84	0	0	301.16	340.967	31.0043	0	2.6	29.8451	0	0	0	0
B2	SA7_Chip	N	12/06/2011	13	285	6.52																					
B2	SA7_Chip	N	13/06/2011	14	308	6.51	70	35	0	0	176.9	20710	0	0	69.77	0	0	608.38	348.517	34.2043	0	0	#REF!	4.22	0	0	0
B2	SA7_Chip	N	15/06/2011	16	349.5	6.53																					
B2	SA7_Chip	N	21/06/2011	22	491.5	6.54	75	35	12.42	0	191.14	30660	0	2.03	0	12.55	0	753.37	686.747	52.8943	361.08	20.8494	1.49	0	0	0	0
B2	SA7_Chip	N	29/06/2011	30	689.5	6.50	75	35	99.55	0	185.83	34050	0	0	47.13	36.35	0	1194.01	780.71	73.27	826.2	2.6194	1.63	0	0	1.8044	0
B3	SA7_Grain	N	31/05/2011	1	4	6.37	60	30	0	0	136.89	10420	0	0	3.43	0	0	0	0	0.28	0	0	6.5	0	0	0	0
B3	SA7_Grain	N	01/06/2011	2	16	7.30	65	30																			
B3	SA7_Grain	N	02/06/2011	3	45	6.73	45	20	0	0.685	180.48	13051	0.09	0.2	11.47	0	4.99	821.31	170.31	19.94	0	0	3.0451	0	0	0.58	0
B3	SA7_Grain	N	03/06/2011	4	69.5	7.02	70	35																			
B3	SA7_Grain	N	04/06/2011	5	91	7.07	65	30	0	2.395	158.16	8900	0.2554	0	21.71	0	0	262.95	170.56	26.7443	0	0	40.0251	0	0	0.27	0
B3	SA7_Grain	N	05/06/2011	6	109.5	6.84	65	30																			
B3	SA7_Grain	N	06/06/2011	7	137	6.79	60	30																			
B3	SA7_Grain	N	08/06/2011	9	183.5	5.23	65	30	0	1.77	201.58	15310	0	1	37.88	0	0	491.7	260.997	33.3943	0	0.54	31.71	10.25	0	0	0
B3	SA7_Grain	N	09/06/2011	10	210.5	5.91																					
B3	SA7_Grain	N	10/06/2011	11	229.5	6.42	75	35	0	3.905	186.08	14240	0	0	43.05	0	0	563.71	260.587	31.4143	0	7.98	#REF!	0	0	0	0
B3	SA7_Grain	N	12/06/2011	13	285	6.46																					
B3	SA7_Grain	N	13/06/2011	14	308	6.54	65	35	0	2.975	189.54	16930	0	1.2702	81.64	0	0	482.72	259.157	35.2243	0	0	11.8951	0	0	0	0

